Journal of Atmospheric and Solar-Terrestrial Physics 71 (2009) 717–728

Contents lists available at ScienceDirect

Journal of Atmospheric and Solar-Terrestrial Physics

journal homepage: www.elsevier.com/locate/jastp

Poker flat radar observations of the magnetosphere–ionosphere coupling electrodynamics of the earthward penetrating plasma sheet following convection enhancements

L.R. Lyons [a,*], S. Zou [a], C.J. Heinselman [b], M.J. Nicolls [b], P.C. Anderson [c]

[a] Department of Atmospheric and Oceanic Sciences, University of California, Los Angeles, Los Angeles, CA 90095-1565, USA
[b] Center for Geospace Studies SRI International, Menlo Park, CA 94025, USA
[c] University of Texas at Dallas, Box 830688 WT15, Richardson, TX 75082, USA

ARTICLE INFO

Article history:
Accepted 28 September 2008
Available online 17 October 2008

Keywords:
Region 2
Plasma sheet
SAPS

ABSTRACT

The plasma sheet moves earthward (equatorward in the ionosphere) after enhancements in convection, and the electrodynamics of this response is strongly influenced by Region 2 magnetosphere–ionosphere coupling. We have used Poker Flat Advanced Modular Incoherent Scatter Radar (PFISR) observations associated with two relatively abrupt southward turnings of the IMF to provide an initial evaluation of aspects of this response. The observations show that strong westward sub-auroral polarization streams (SAPS) flow regions moved equatorward as the plasma sheet electron precipitation (the diffuse aurora) penetrated equatorward following the IMF southward turnings. Consistent with our identification of these flows as SAPS, concurrent DMSP particle precipitation measurements show the equatorial boundary of ion precipitation equatorward of the electron precipitation boundary and that westward flows lie within the low-conductivity region between the two boundaries where the plasma sheet ion pressure gradient is expected to drive downward R2 currents. Evidence for these downward currents is seen in the DMSP magnetometer observations. Preliminary examination indicates that the SAPS response seen in the examples presented here may be common. However, detailed analysis will be required for many more events to reliably determine if this is the case. If so, it would imply that SAPS are frequently an important aspect of the inner magnetospheric electric field distribution, and that they are critical for understanding the response of the magnetosphere–ionosphere system to enhancements in convection, including understanding the earthward penetration of the plasma sheet. This earthward penetration is critical to geomagnetic disturbance phenomena such as the substorm growth phase and the formation of the stormtime ring current. Additionally, for one example, a prompt electric field response to the IMF southward turnings is seen within the inner plasma sheet.

1. Introduction

Vasyliunas (1968) concluded that the plasma sheet moves inward during geomagnetically active periods as a result of inward plasma motion driven by the cross-tail electric field. This inward motion is a response to enhanced convection (Elphic et al., 1999; Korth et al., 1999), and is a critically important aspect of the dynamics of the plasma sheet. It can lead to strong increases in plasma pressure within the inner magnetosphere and the associated stretching of the geomagnetic field, which constitute the growth phase of substorms (Lyons 2000, and references therein). Under strongly enhanced convection conditions, the earthward penetration of the plasma sheet provides the source for the stormtime ring current, as inferred from observations (Korth et al., 2000; Wang et al., 2008) and is often incorporated into ring current models (e.g., Kozyra et al., 1998; Chen et al., 2007).

However, the earthward penetration of the plasma sheet depends strongly on the coupling between the plasma sheet and the ionosphere, since this coupling significantly affects the structure of the nightside convection electric field. An enhancement in convection leads to enhanced electric fields within the plasma sheet. These electric fields extend earthward of the preexisting location of the plasma sheet, where they are referred to as penetration electric fields and are particularly well observed within the dayside equatorial ionosphere because of their effects on the equatorial electrojet (e.g., Wolf, 1983; Wolf et al., 2007; Fejer and Scherliess, 1995). An enhancement of electric fields on the night side is required for the plasma sheet to move earthward

* Corresponding author.
E-mail addresses: larry@atmos.ucla.edu (L.R. Lyons), sha@atmos.ucla.edu (S. Zou), craig.heinselman@sri.com (C.J. Heinselman), michael.nicolls@sri.com (M.J. Nicolls).

1364-6826/$ - see front matter © 2008 Elsevier Ltd. All rights reserved.
doi:10.1016/j.jastp.2008.09.025

from its previous location. However, associated with this earthward motion is a build up of plasma pressure and plasma pressure gradients. This enhances the Region 2 (R2) currents, which are driven by the pressure gradients and connect the plasma sheet with the ionosphere. In order for these currents to flow in the ionosphere, electric fields form within the ionosphere, and these electric fields map back up to the magnetosphere and tend to shield the region earthward of the plasmasheet. Thus as the plasma sheet moves earthward and plasma pressure increase, shielding gradually develops, substantially modifying the plasma sheet electric field and the transport of plasma sheet particles (e.g., Wolf et al., 2007, and references therein).

The transport and energization of particles that is associated with the earthward penetration of the plasma sheet following an enhancement in convection is thus strongly influenced by the electrodynamical coupling with the ionosphere. This electrodynamics is accessible for study using incoherent scatter radars that can measure plasma flows and ionospheric electron densities as a function of latitude and time within the auroral zone. In the present paper, we use data from the new Poker Flat Advanced Modular Incoherent Scatter Radar (PFISR) to evaluate aspects of the electrodynamical response to enhancements in convection.

We use the densities measured by PFISR to evaluate the inner edge of the diffuse aurora and its temporal variations. The inner edge of the diffuse aurora gives the equatorward boundary of enhanced conductivities within the auroral ionosphere. Because pitch-angle diffusion of the electrons into the ionosphere is responsible for the diffuse aurora, the equatorward edge of the diffuse aurora should also approximately track the time variations of the inner edge of the plasma sheet electron population. By examining together the temporal motion of this inner edge and the ionospheric flows that are measured by the radar, we are able to evaluate the ionospheric electric field evolution relative to the time-dependent motion of the inner edge of the plasma sheet and the associated region of enhanced ionospheric conductivities.

An important aspect of the response that we find in the data is the formation and equatorward motion of a region of strongly enhanced flows lying just equatorward of the equatorial boundary of the diffuse aurora. Such flows, located in the low-conductivity region equatorward of the equatorward boundary of the auroral oval (Anderson et al., 1993), are now referred to as sub-auroral polarization streams (SAPS) (e.g., Foster and Burke, 2002). They are known to occur in the region between the equatorward boundaries of plasma sheet ion precipitation and of plasma sheet electron precipitation at MLTs where the ion boundary is equatorward of the electron boundary (Anderson et al., 2001). It has been proposed that SAPS are driven by the plasma sheet pressure gradients that lead to R2 currents, but in the region equatorward of the plasma sheet electrons where ionospheric conductivities are low so that large electric fields are required to maintain current continuity within the ionosphere (Southwood and Wolf, 1978). Consistent with this proposal, the equatorward boundary of SAPS has been found to be coincident with the equatorward boundary of the region of downward R2 field-aligned currents, as well as with the equatorward boundary of plasma sheet ions (Anderson et al., 2001). We do not address in this study the narrow more intense enhancements of flows have been found within SAPS flow regions, which have been referred to as "polarization jets" (Galperin et al., 1974) or "sub-auroral ion drifts (SAIDs)" (Spiro et al., 1979).

In this initial use of PFISR observations to evaluate aspects of the electrodynamical response to enhancements in convection, we focus on the response to relatively abrupt southward turnings of the IMF, which are expected to lead to an abrupt increase in convection, and consider two of the cases that have occurred during the periods of radar runs.

2. Radar mode

PFISR is located at 65.4° magnetic latitude near Fairbanks, Alaska. It is a modern phased array radar with the ability to steer on a pulse-to-pulse basis, allowing essentially simultaneous measurements in multiple look directions since typically hundreds to thousands of pulses are integrated to form a single measurement (Heinselman and Nicolls 2008). The radar operation mode selected for our studies of ionosphere–plasma sheet electrodynamical coupling consists of 13 beam directions as shown in the geomagnetic longitude and latitude plane in Fig. 1. This configuration of beams has been chosen to cover as large a distance in the magnetic north–south direction as possible. Some of our runs have been in a similar "world-day" mode, which is the

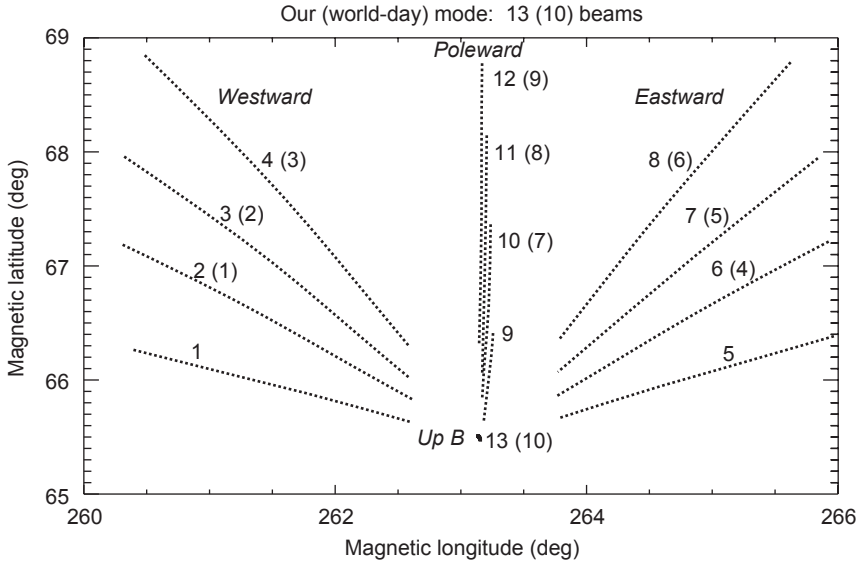

Fig. 1. Directions of radar beams selected for our studies of ionosphere–plasma sheet electrodynamics in the geomagnetic longitude and latitude plane. Configuration chosen to cover as large a distance in the magnetic north–south direction as possible. Some of our runs have been in the "world-day" mode, which is the same as our mode except for the lack of three lowest latitude beams. Beam numbers in parenthesis are for the world-day mode.

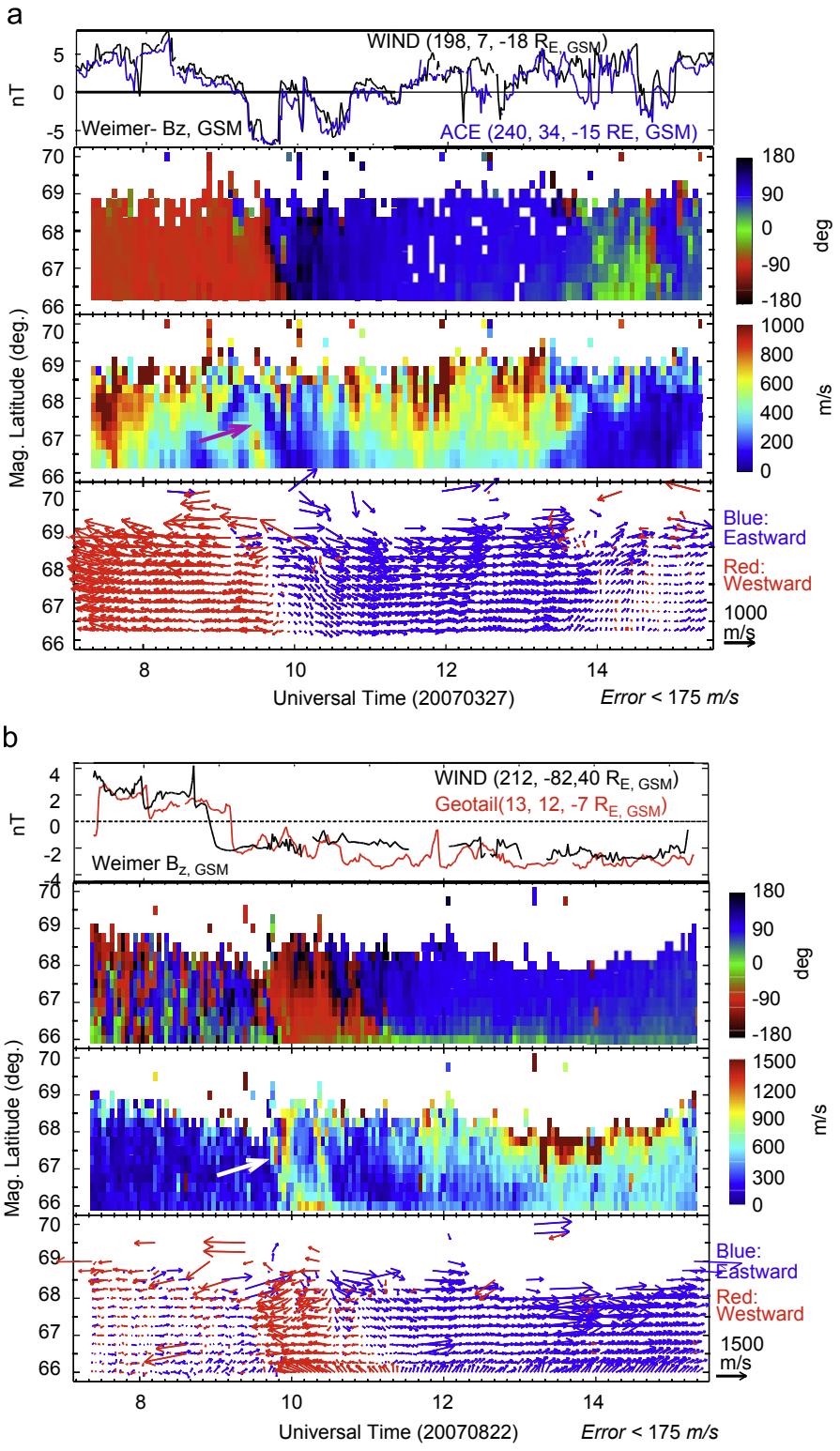

Fig. 2. (a) Overview of the radar observations of F-region flow velocities from the ~8 h run approximately centered on midnight MLT (1115 UT) on 27 March 2007. Time resolution of the data shown is ~4 min. Second and third panels in the figures give color displays of the direction and magnitude, respectively, of the flows versus magnetic latitude and UT, and the bottom panel shows each flow vector. Only data with an error < 175 m/s are shown. Upper panel shows the IMF B_z in GSM from all available monitors as Weimer-mapped to $x = 17R_E$ along the Earth–Sun line. Equatorward-moving region of enhanced flows in response the IMF southward turning is identified by a heavy arrow within the flow magnitude panel. (b) Same as (b), except for 22 August 2007 and time resolution of the data shown is ~3 min.

same as that shown in Fig. 1 except for the exclusion of the low-latitude beams 1, 5, and 9. In Fig. 1, beam numbers in parentheses are for the world-day mode. Beams 1–4 (1–3) point to the northwest, 5–8 (4–6) to the northeast, 9–12 (7–9) directly to the north, and 13 (10) directly up the local magnetic field line.

Vector velocities within the F-region are calculated as a function of latitude along the radar magnetic meridian from the multiple line-of-sight measurements within each latitude bin under the assumption that longitudinal variations within the radar field-of-view can be neglected. In addition, some constraints

are placed on the magnitude of the parallel drifts based on long-term observations. These drifts are dominated by neutral wind effects and are typically less than ± 15 m/s. Details of the radar transmission scheme and methodology of velocity vector calculation are described in Heinselman and Nicolls (2008). Generally, long pulses are used for F-region measurements and alternating code pulses for E-region measurements because of the much different scale heights of the two regions. The latter provides much higher range resolution than the former in the E-region. We use only the long pulse data in this paper. In the future, we plan to obtain F-region velocity vectors along two magnetic meridians, one to the west and one to the east of the radar meridian, which will give improved information on longitudinal variations. Note that, unlike for steerable radars, the integration time used for the velocity measurements is selected when post-processing the data and is not limited by the scan time.

3. Observations

Overviews of the radar observations of F-region flow velocities from ~8 h runs approximately centered on midnight MLT (1115 UT) on 27 March 2007 and 22 August 2007 are shown in Figs. 2a and b, respectively. The time resolution of the data shown is ~4 (3) min for the data on 27 March (22 August). The second and third panels in the figures give color displays of the direction and magnitude, respectively, of the flows versus magnetic latitude and UT, and the bottom panels shows each flow vector. Observations extend down to 66° latitude on 27 March when the radar was in the world-day mode, and to 65.75° latitude on 22 August when the radar was in our operation mode. The data becomes quite noisy above ~69° latitude because of the decrease in the accuracy of the line-of-sight flows with increasing range and as the density decreases above the F2 peak, and only data with an estimated error <175 m/s are shown. Additionally, the longitude separation of the beams increases with increasing latitude, which could introduce increasing error due to the neglect of possible longitudinal variations when calculating the flow vectors. The effective latitude range of valid measurements is ~3°.

For reference, the z-component B_z of the interplanetary magnetic field (IMF) is show in the upper panels of each figure as Weimer-mapped (Weimer et al., 2003; Weimer, 2004) to $x = 17R_E$ along the Earth–Sun line. On 27 March, we focus on the response to the southward turning of the IMF that impacted the magnetosphere shortly after 0920 UT as seen by both WIND and ACE. After the southward turning, B_z remained near -5 nT for ~25 min and then abruptly turned northward (leading to a substorm onset at 0946 UT, as clearly seen in optical, geosynchronous particle, and ground magnetic observations). On 22 August, a southward turning was seen in both the WIND and Geotail observations, which was followed by a prolonged period of $B_z \sim -2$ nT. The impact of the southward turning was at ~0915 UT, based on the Geotail observations (WIND was too far away from the Earth–Sun line to provide reliable timing information). These are both non-storm intervals.

The response to the above southward turnings is seen as a region of enhanced flows with speeds $\gtrsim 500$ m/s that is initially seen at the highest latitudes and then moves equatorward over a period of ~5–10 min. The region is identified by a heavy arrow within the flow magnitude panel for both days, and can also been seen in the flow vectors. Fig. 3 shows the flow vectors with 1 min time resolution for 1 h time intervals that include the time of the flow enhancement. These equatorward-moving regions of enhanced flows are particularly clear in the color plots of the line-of-sight velocity versus altitude and UT for the individual beams that are shown in Figs. 4a and b for $2\frac{1}{2}$ h time periods approximately centered on the flow enhancements of interest. Here the individual beams are displayed in a pattern similar to Fig. 1, westward-looking beams on the left, eastward-looking beams on the right, and poleward-looking beams in the center. The highest elevation beams are in the bottom panels, with the successively lower elevation beams stacked in the panels above. Note that increasing radar beam altitude corresponds to increasing latitude, as illustrated by the beams paths in Fig. 1. Thus, the individual plots can be viewed as giving flows versus latitude, with the latitude range being covered decreasing with increasing beam direction angle relative to magnetic north. Both altitude and magnetic latitude are shown along the vertical axes. Positive velocities indicate flows directed away from the radar.

The equatorward-moving flow regions can be seen in the westward (eastward) looking beams as bands of enhanced flows moving away from (towards) the radar. While the flows are

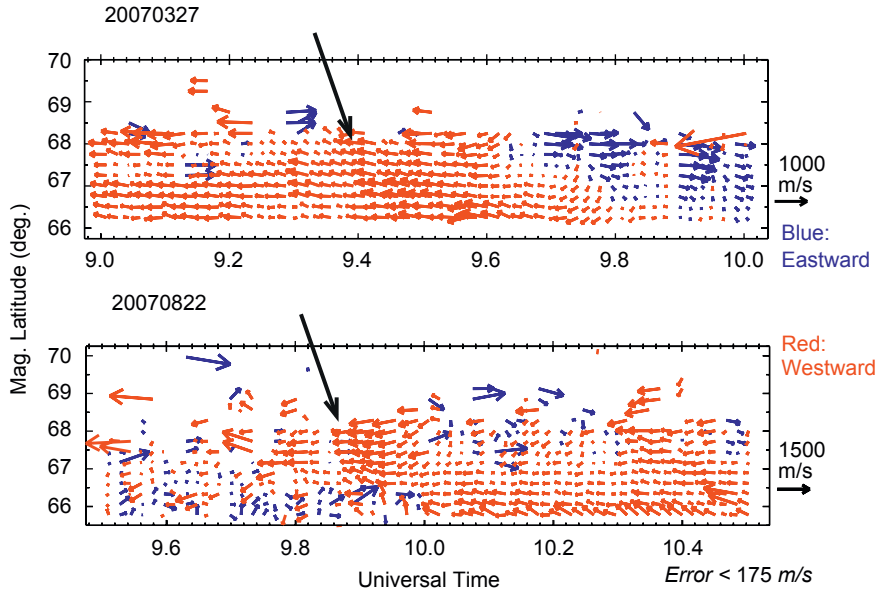

Fig. 3. F-region flow vectors with 1 min time resolution for 1 h time intervals that include the time of the flow enhancement on 27 March and 22 August 2007.

approximately westward, there are small north–south components to the flows as indicate by the flows seen by the poleward-looking beams, which are in the center column of the figures. Note that above ~180 km altitude, the plasma can be considered collisionless so that flows are primarily from the electric field drift velocity, so that a westward flow component indicates a poleward-directed component of the electric field. At lower altitudes, the flow velocity and direction may not be representative of electric field drift due to the increasing effects of neutral winds and collisions with decreasing altitude (e.g., Heinselman and Nicolls, 2008).

On 27 March, the flow enhancement in response to the southward turning of the IMF is first seen at ~0920 UT. Several equatorward-moving regions of enhanced flows can be seen prior to this time, but the earlier flows do not stand out as much from the background and are not associated with the earthward motion of the plasma sheet that is discussed later. On 22 August, the flow enhancement can be seen as two enhancements separated by ~30 min as measured by beams 3 and 4, and the enhancement stands out very clearly from any other flow signatures seen during the radar run. Line plots of the line-of-sight velocities from the westward and poleward-looking beams for $1\frac{1}{2}$ h intervals including the flow enhancements are shown on the left side of Figs. 5a and b. (The westward-looking beams are shown rather than the eastward-looking beams since they have a poleward component to their look direction and are thus directed closer to the direction of the flows.) For each beam, flows are shown at locations equally spaced in latitude, except only two locations are shown for beams 1 and 9 on 22 August because of the small latitude range covered by these beams. Each location is shown by a different color, and the dashed lines of the same color indicate zero line-of-sight speed and are drawn at the latitude of the flow measurement.

Vertical dashed lines in each panel identify the estimated time of the initiation of effects in the ionosphere of the IMF southward turning. For 27 March, the westward-looking beams show an increase in flow speed initiating very close in time to the identified time of the southward turning at all locations displayed. There are other variations in the flows that occur at earlier times, but the increase at the time of the southward turning is seen essentially simultaneously at all locations and the increase is far more persistent than the earlier flow variations. Some evidence of a flow response can also be seen in the flows measured by the poleward-looking beams. Similarly, on 22 August, evidence of a persistent flow increase can also be seen in the flows measured by the westward-looking beams, particularly beams 2 and 3, at all locations. On this day, the first flow enhancement initiated ~20 min after the estimated impact time of the IMF southward turning on 22 August. This delay may be related to the magnitude of the IMF B_y (not shown), which affects the strength of convection as well as does B_z. B_y and abruptly decreased from 3 nT to near 0 nT at the time of the southward turning and then gradually increased to ~2 nT over the next ~15 min. Also, as discussed later, the E-region electron densities seen by the radar show that these electric field enhancements extended equatorward of the region of plasma sheet electron precipitation, so that lower latitude flow increases on 27 March are evidence for electric fields rapidly penetrating earthward of the nightside plasma sheet in association with the southward turning.

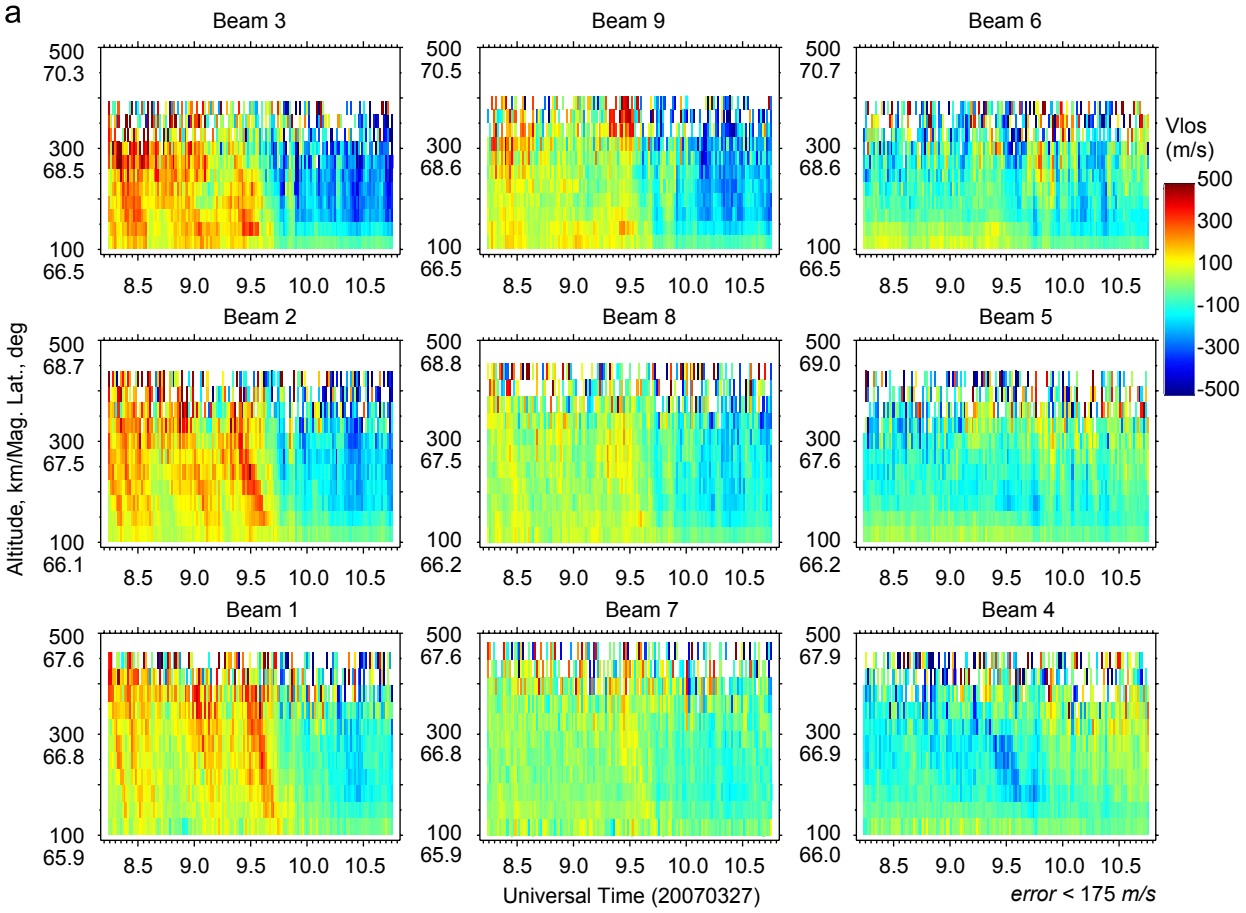

Fig. 4. (a) Color plots of line-of-sight velocity versus altitude and UT for the individual radar beams on 27 March 2007 for a $2\frac{1}{2}$ h time period approximately centered on the flow enhancement of interest. Geomagnetic latitude is also indicated along the vertical axis. Positive velocities indicate flows directed away from the radar. Only data with an error <175 m/s are shown. (b) Same as Fig. 4a, except for 22 August 2007.

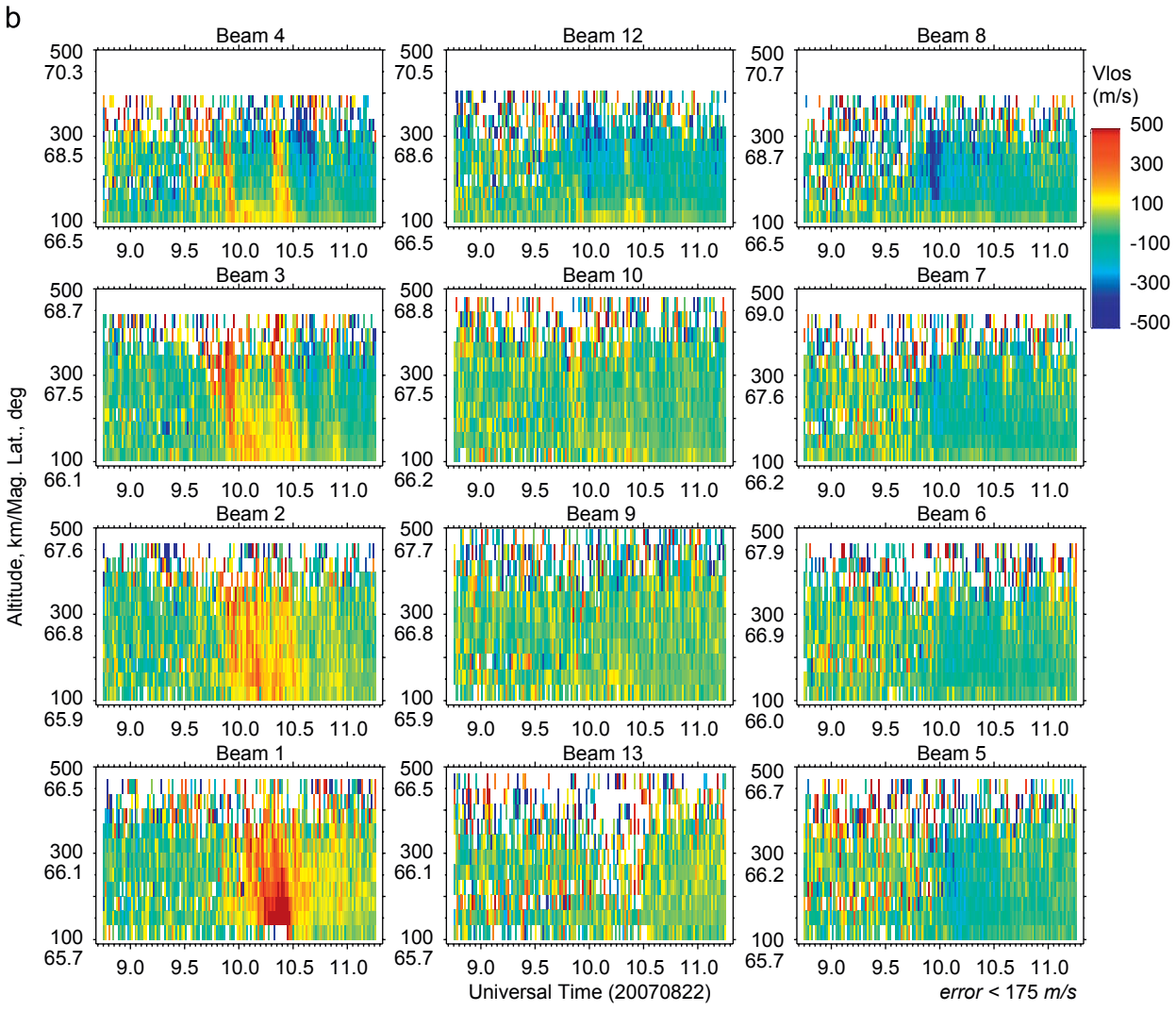

Fig. 4. (*Continued*)

Very clearly seen in Fig. 5, particularly in the westward flows, is that the flow speed increases that follow the southward turnings reach a peak of a few 100 m/s and then decrease substantially and rather abruptly. Circles are drawn on the flow speed lines in Figs. 5a and b at the times when the flow enhancement peak, and it can be seen very clearly that the peaks in the flow speeds move equatorward with time. The equatorward motion can be seen both in the flows within each panel and by comparing the flows for the different westward or poleward-looking beams at the same altitude. This peak is unambiguous on 27 March. On 22 August, the peaks of the two major flow enhancements are identified for the four most poleward looking of the westward and poleward-looking beams (beams 3, 4, 11, and 12). Also, for the first enhancement, there is evidence for two flow peaks separated by a few min at latitudes above 67°. Only the first of these enhancements is identified. Below 67°, these two peaks become indistinguishable. Only the first of the major flow enhancements is clear in the observations from the less poleward-looking beams 2 and 10, and a peak is not identified for the lowest latitude beams, an interesting feature that is discussed later. At the higher latitudes, the reduction in flow speed after the peak leads to eastward flows. This leads to a flow direction reversal as a function of latitude, which can be seen clearly in the flow direction panels in Fig. 2a and b as a transition from red to blue with increasing latitude and in the flow vectors in Fig. 3. This flow reversal, which lies well equatorward of the open-closed field line boundary, is known as the Harang reversal (or Harang discontinuity) (Erickson et al., 1991).

4. The SAPS response

We now address the question of what causes the equatorward-moving flow peaks and the nature of their relationship to the response of the plasma sheet following enhancements in convection. To do this, we examine the radar measurements of electron density, which are plotted on the right side of Figs. 5a and b for the same beams and locations as the line-of-sight flows on the left side of the figures. For both cases, it can be seen that, following the southward turnings, the electron densities show an abrupt increase within the E-region by a factor ~3–10. Such an increase is a response to auroral electron precipitation and thus identifies a transition to a region of substantial auroral electron precipitation. The enhancement can be discerned well up into the lower F-region, and can clearly be seen to move equatorward with time. After the densities increase, they remain elevated at each location throughout the following ~1 h time period shown in Figs. 5a and b. The only exceptions are a few short variations at the lowest altitude in beams 3 and 9 on 27 March, which may result from more energetic (>1 keV (Rees, 1963)) electrons associated with

auroral arcs, and the densities seen on 22 August at latitudes $<66^{\circ}$ by beams 1 and 9, which did not increase to the densities reached at the higher latitudes until ~10 UT or later.

These density increases are the expected response from the equatorward motion of the broad region of diffuse aurora electron precipitation resulting from the earthward motion of plasma sheet electrons. To examine how the equatorward-moving flow peaks relate to the equatorward motion of the precipitation resulting from the equatorward-moving plasma sheet, we have placed circles that identify the times of the velocity peaks on the corresponding curves of the electron densities. This allows us to determine the timing of the velocity peaks relative to that of the ionospheric density increases. For 27 March, it can be seen that there was a remarkable coincidence between the times of the velocity peaks and the times of initiation of the increase in densities. The association is nearly as good for the first velocity

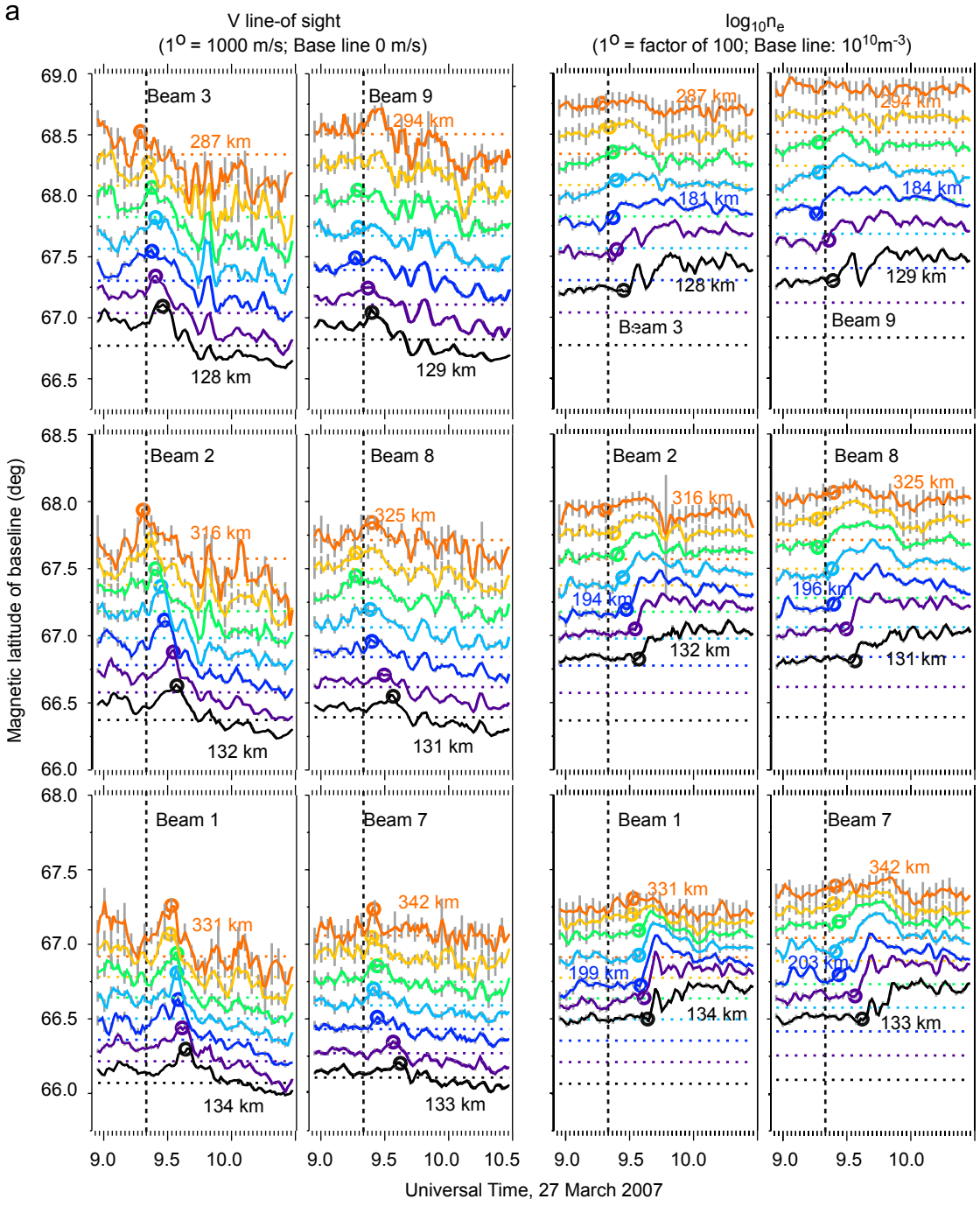

Fig. 5. (a) *Left panels*: line plots of 3-point running averages of the line-of-sight velocities from the westward and poleward-looking beams for a $1\frac{1}{2}$ h interval that includes the flow enhancements on 27 March 2007. Velocities from the different selected locations are shown by different colors in each panel, and the dashed lines of the same color indicate zero line-of-sight speed and are drawn at the latitude of the flow measurement. Positive velocities indicate flows directed away from the radar. Circles are drawn on the flow speed lines at the times of the flow enhancement peaks. *Right panels:* radar measurements of electron density for the same beams and locations as the line-of-sight flows on the left side of the figures. Dashed lines of the same color indicate a density of 10^{10} m^{-3}. Circles identifying the times of the velocity peaks are drawn on the corresponding curves of electron density. *All panels:* vertical dashed lines identify the estimated time of the impact on the ionosphere of the IMF southward turning, and error bars are shown every three points. (b) Same as Fig. 2b, except for 22 August 2007.

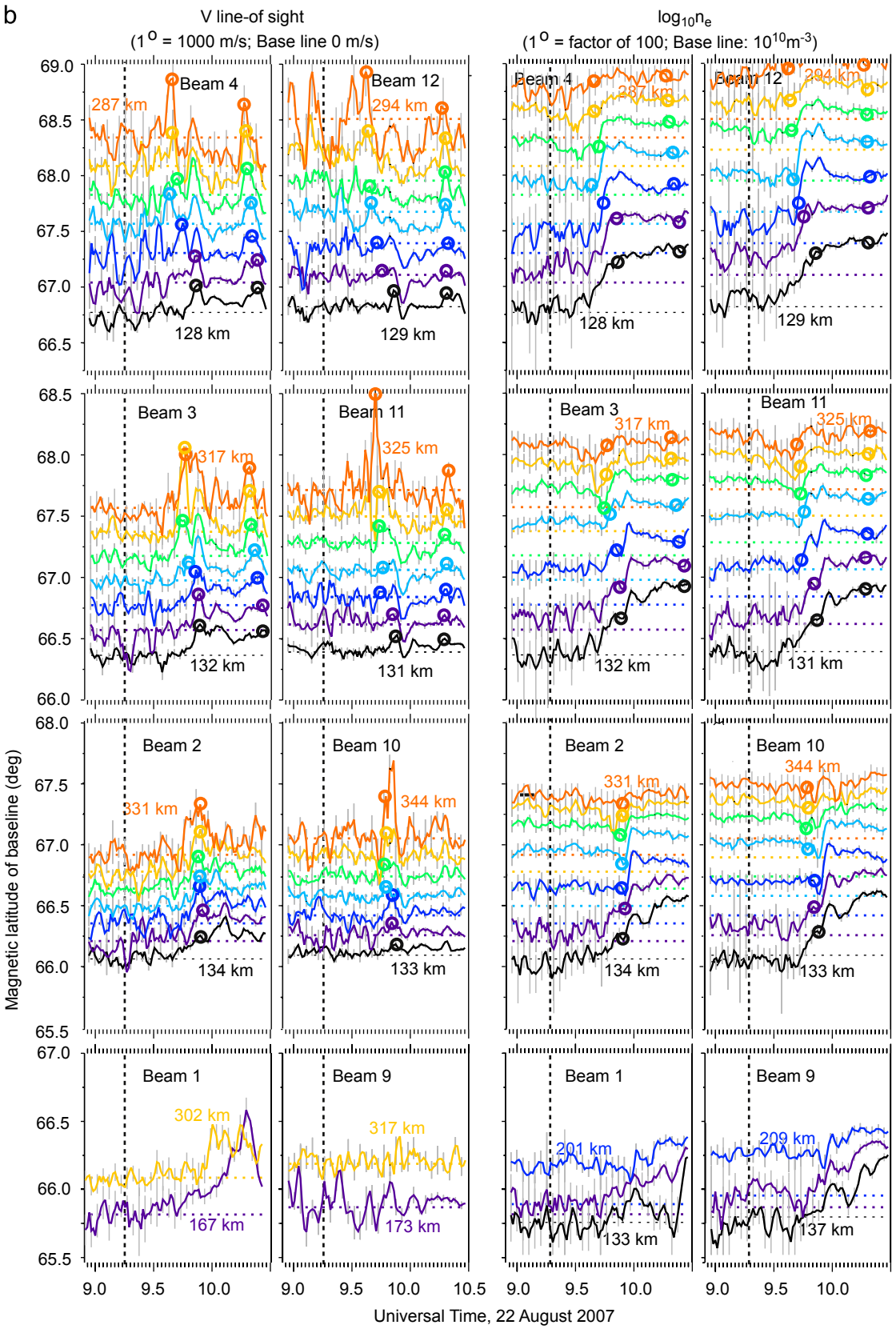

Fig. 5. (*Continued*)

enhancement on 22 August. Such an association was not seen, however, for the second velocity enhancement on 22 August, which occurred well after the southward turning of the IMF.

The spatial relationship seen in the PFISR observations between the enhanced flows and the electron densities is expected if the enhanced flows equatorward of the plasma sheet

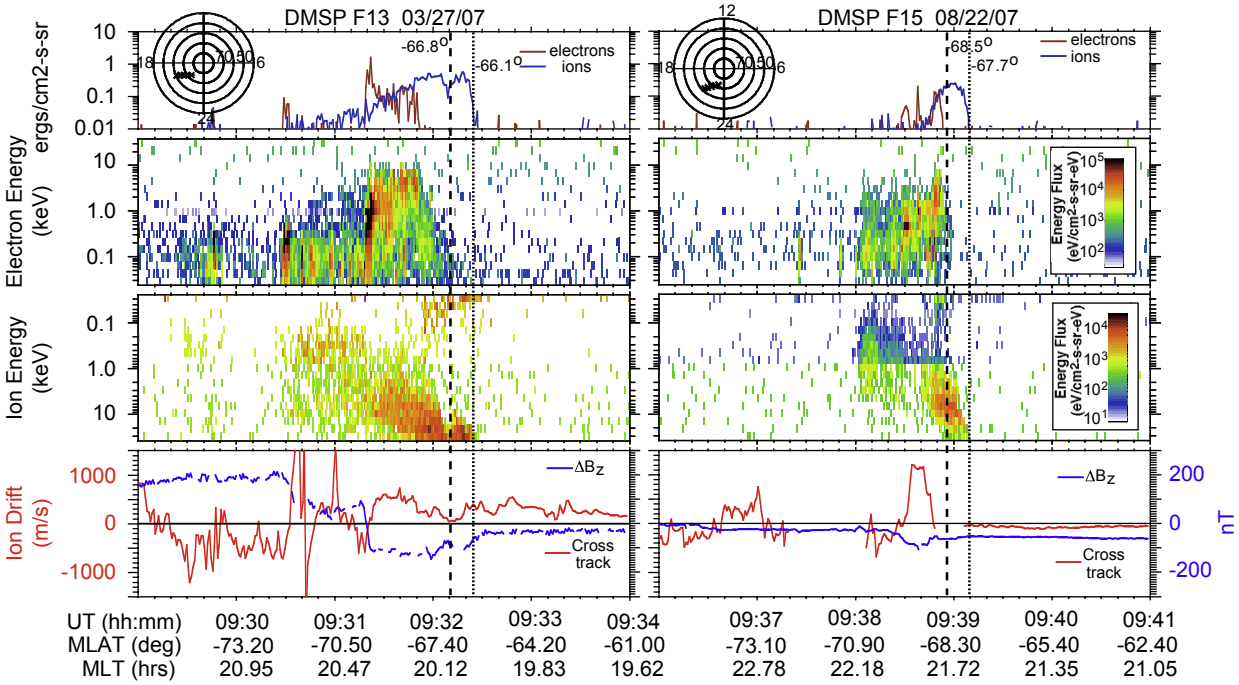

Fig. 6. DMSP observations of 30 eV–30 keV precipitating electrons and ions during passes soon after the IMF southward turnings on 27 March and 22 August. Also shown for each pass are the total measured precipitating electron and ion fluxes, the cross-track plasma flow speed (positive values indicating westward flow), and the horizontal magnetic field perturbation in the direction nearly normal to the spacecraft trajectory (an increase towards lower latitudes indicating downward field-aligned currents). Dashed and dotted lines indicate the approximate location of the equatorward edge of observable plasma sheet electron and ion precipitation, respectively.

electron precipitation are SAPS. If this is the case, then plasma sheet ions should extend to the field line region of enhanced flows that lie equatorward of the region of precipitating plasma sheet electrons. Ion precipitation cannot be observed by the radar. However, we are fortunate that there were passes of the low-altitude Defense Meteorological Satellites Program (DMSP) spacecraft over the Southern Hemisphere auroral zone near the longitude of PFISR at times soon after the southward turnings of the IMF, which can be used to evaluate SAPS and their relation to precipitation features (e.g., Anderson et al., 2001). Fig. 6 shows the DMSP observations of 30 eV–30 keV precipitating electrons and ions during such passes, one on 27 March and the other on 22 August. Also shown for each pass are the total measured precipitating electron and ion fluxes, the cross-track plasma flow speed (positive values indicating westward flow), and the horizontal magnetic field perturbation in the direction nearly normal to the spacecraft trajectory (an increase towards lower latitudes indicating downward field-aligned currents). Dashed and dotted lines indicate the approximate locations of the equatorward edge of observable plasma sheet electron and ion precipitation, respectively.

Observations from DMSP F13 that crossed the equatorial boundary of plasma sheet precipitation at ~0932 UT on 27 March are shown on the left side of Fig. 6. The crossing of F13 was at ~20.1 MLT, about 2 h earlier than the location of PFISR. The particle observations clearly show that the equatorward boundary of the ion precipitation was substantially equatorward of that of electrons, as required for the formation of SAPS at the time of the flows measured by PFISR that we have inferred to be SAPS. While we do not expect precise agreement between the magnetic latitudes of features observed in the different hemispheres, the inner boundary identified in the figure for electrons is within ~0.5° in latitude of the ~66.3° inferred from the radar measurements at 0935 UT and the ~0.7° latitudinal difference between the electron and ion boundaries is sufficient for SAPS to account for the flows equatorward of the electron precipitation boundary observed by the radar at this time. Additionally, the spacecraft observed westward flows equatorward of the inner edge of the electron precipitation, consistent with the PFISR observations, and the magnetic perturbation indicates downward field-aligned current within the SAPS region. Westward flows were also seen well equatorward of the plasma sheet, which could result from penetration electric fields associated with the IMF southward turning ~12 min earlier.

The pass of DMSP F15 shown in the upper right portion of Fig. 6 shows the equatorward boundary of the electron plasma sheet at −68.5° latitude at 0939 UT on 22 August at an MLT about ~0.5 h earlier than PFISR at that time, which is nearly the same latitude as the boundary seen by PFISR at this time. Also, as on 27 March, the observations clearly show that the equatorward boundary of the ion precipitation was substantially (0.8°) equatorward of that for electrons, as required for the formation of SAPS. Thus, for both days, the simultaneous DMSP measurements show that inner edge of the plasma sheet ions was equatorward of the inner edge of precipitating electrons, which lends strong support to our inference that the duskward flows seen by the radar equatorward of the electron plasma sheet were indeed SAPS. Flow observations were not available within the SAPS region on this DMSP orbit because of very low ionospheric densities. Also, the downward field-aligned current was quite weak in this region, which could be due to the IMF being more weakly southward than for the 27 March event.

The observations in Fig. 5a show that on 27 March the SAPS flow peaks and E-region density increases continued to move equatorward to the lowest latitude of the radar observations (66.1°) by 0938 UT. The speed of equatorward motion seems to have decreased as the structure moved equatorward, as can be seen by the horizontal spacing of the circles that identify the velocity peaks. However, the plasma sheet electron precipitation clearly penetrated to the lowest latitude, implying that the SAPS

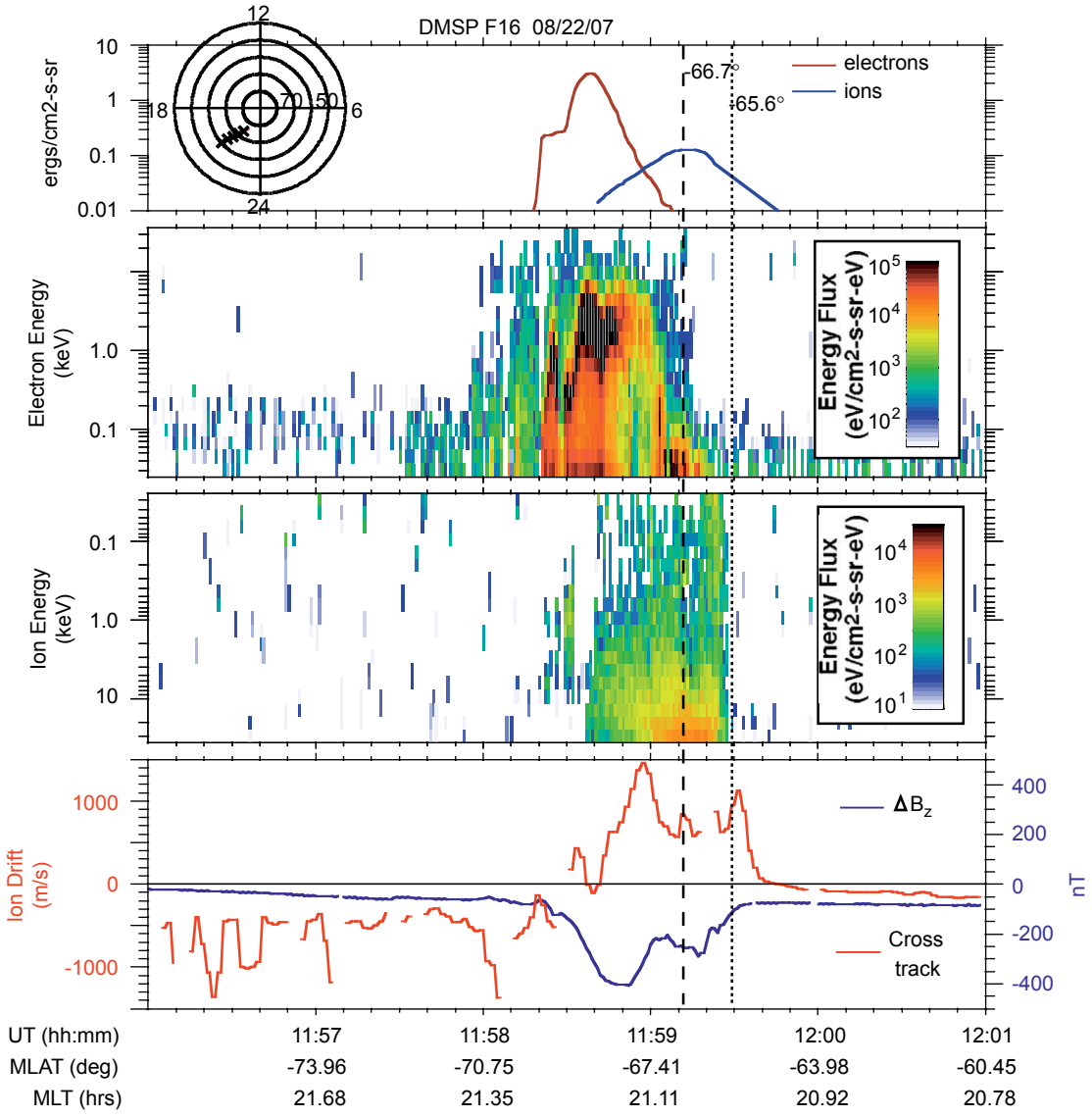

Fig. 7. Same as Fig. 6, except for a DMSP pass 2 h 20 min after the pass in the upper right portion of Fig. 6.

flows moved to latitudes lower than those observed by the radar ~20 min after the IMF southward turning.

On 22 August, the SAPS region moved equatorward as on 27 March, but the flows did not substantially decrease after increasing at latitudes of 66.1° and below. Also the E-region densities did increase as quickly to the values reached on 27 March in this region. These differences in the flows and densities can be seen by comparing the black curves, which are at 66.1° latitude, in the bottom panels of Fig. 5a to the same curves in the second to bottom panels in Fig. 5b. Additionally, on 22 August the flow increases and subsequent flow decreases seen by beam 1 are considerably delayed from when they occurred at higher latitudes. For example, flow decreases are not seen in the flows observed by beam 1 until ~1015 UT. Furthermore, the densities measured by beams 1 and 9 do not show the increases to the levels seen at higher latitudes until ~1015 UT. This suggests that the plasma sheet and SAPS region did not penetrate to ~66.1° and below as rapidly on 22 August as on 27 March, which may be related to the IMF being not as strongly southward on 22 August.

It seems plausible that the SAPS region seen by the radar on 22 August would persist during the ensuing prolonged period of southward IMF. This possibility cannot be evaluated using the PFISR data because the SAPS moved equatorward of the PFISR field of view after ~1015 UT, but evidence for such persistence can be seen in the DMSP F16 pass at 1159 UT shown in Fig. 7, which was ~2 h 45 min after the southward turning and during the period of prolonged southward IMF that followed that southward turning. This shows the equatorward boundaries of the plasma sheet electron and ion precipitation to be ~2° equatorward of where they were on the 2 h 20 min earlier F15 pass in the upper right portion of Fig. 6, although the later pass was ~50 min earlier in MLT, and westward flows and downward field-aligned currents are seen within the region between the two equatorward boundaries. These observations are consistent with there being a persistent SAPS region between the boundaries during prolonged periods of steady southward IMF, as has been found to be generally the case during disturbed conditions (Foster and Vo, 2002). Also, that the equatorward boundaries did not move very far equatorward of where they were earlier suggests the possibility that there may be a limit as to how far equatorward the SAPS and plasma sheet can penetrate during a period of steady southward IMF. It would be interesting to test both possibilities with more thorough analysis.

Finally, it is important to note that not all equatorward-moving flow enhancements are SAPS. For example, the second major flow enhancement on 22 August, first seen at 1010 UT, is not SAPS since it occurred within the region of enhanced E-region densities associated with plasma sheet electron precipitation. Such flows are expected from the mapping of localized flow bursts that occur in the tail (Angelopoulos et al., 1994, 1996), which have been associated with auroral enhancements (e.g., de la Beaujardière et al., 1994; Lyons et al., 1999; Zesta et al., 2006). PFISR can be used to evaluate such flow bursts within the plasma sheet and their relationship to observations of auroral enhancements (see Zou et al. (2008) for an initial study of this relationship).

5. Discussion and conclusions

We have used PFISR observations associated with two relatively abrupt southward turnings of the IMF to provide an initial evaluation of aspects of the electrodynamical response of the plasma sheet–ionosphere system to enhancements in convection. Our analysis demonstrates the use of the fast temporal resolution afforded by PFISR for such studies and shows important features of the response.

Our major result is that SAPS are a significant part of this response. In particular, we have found SAPS flow regions moving equatorward as the plasma sheet electron precipitation (the diffuse aurora) penetrates equatorward following the IMF southward turnings. At a given latitude, the SAPS flows equatorward of the region of the plasma sheet electron precipitation are seen to increase with time as the precipitation region moves closer, and the flows are seen to peak just when the equatorward boundary of precipitation effects is first seen in the E-region densities at the latitude. The flows then decrease with the increase in E-region densities (and thus of conductivity) as the electron precipitation moves further equatorward. The peak of the SAPS flows moved equatorward at a speed of ~120 m/s for both cases presented here, which is comparable to the ~150 m/s seen by Foster et al. (2004) for the poleward boundary of a SAPS region during a stormtime period. Also, the two peaks separated by a few min at latitudes above 67° for the SAPS flows on 22 August could be related to equatorward propagating wavelike structures seen by Foster et al. (2004).

Concurrent DMSP particle precipitation measurements in the Southern Hemisphere show quite clearly that the equatorward boundary of the plasma sheet ion precipitation was equatorward of the equatorial boundary of electron precipitation, consistent with the existence of enhanced westward SAPS flows lying within the region between the equatorward boundaries of the plasma sheet electron precipitation and ion precipitation where the conductivities are expected to be low. This is the region where the azimuthal pressure gradient of the plasma sheet ions is expected to drive downward R2 currents, and evidences for these downward currents are seen in the DMSP magnetometer observations.

While we have so far only examined in detail the two events presented here, we have found evidence for such equatorward-moving SAPS in the observations from 12 of the 22 radar runs that we have so far looked at. However, detailed analysis will be required for many more events to reliably determine how common is the SAPS response seen in the examples presented here. Such analysis will also be required to determine the extent to which the SAPS response varies with differences in conditions, such as IMF B_y and B_z, solar wind density and velocity, and preceding geomagnetic conditions.

Previous studies have established that SAPS can be an important contributor to the overall distribution of inner magnetospheric electric fields (Anderson, 2004; Goldstein et al., 2005), and SAPS have previously been observationally related to substorms (Anderson et al., 1993] and storms (Yeh et al., 1991; Rowland and Wygant, 1998; Burke et al., 1998). They have been observed to occur at lower latitude with increasing K_p index during disturbed conditions (Foster and Vo, 2002) and to have significant temporal variability (Oksavik et al., 2006). While weaker than the SAPS flows typically seen during storms, the data shown here suggest that SAPS may generally be a fundamentally important part of the response of the plasma sheet–ionosphere system to enhancements of convection. If future analyses show that this is generally true, it would imply that SAPS are frequently an important aspect of the inner magnetospheric electric field distribution and are critical for understanding the response of the magnetosphere–ionosphere system to enhancements in convection.

The observations during the two events presented here do not show evidence for substantial equatorward flows following the two southward turnings of the IMF, contrary to what would be expected from a penetration electric field at the MLTs of the observations. However, equatorward flow within the ionospheric mapping of the plasma sheet is required for the plasma sheet to move equatorward as observed. In fact, the observations show that the SAPS flows may have had a small poleward component in addition to their predominant westward component. The observations presented here were at ~22–23 MLT, and so it is possible that the required equatorward flows occurred closer to midnight and/or at early morning MLTs. This would imply that protons reach the MLTs of the PFISR observations presented here via magnetic drift. It will be interesting to examine PFISR observations for events at later MLTs to see if equatorward drifts can be seen.

Also, we have suggested that the observations presented here are consistent with the penetration of the plasma sheet continuing to increasingly low latitudes with increasingly strong southward IMF B_z, and with a cessation of further penetration but continuation of SAPS during periods of prolonged steady southward IMF. It should be interesting to check these possibilities, though it is likely that this would require more than only PFISR observations because of the penetration of SAPS and the plasma sheet to latitudes lower than the PFISR field-of-view.

Finally, to within the few minute limit of our ability to determine the impact time of the southward turnings on the magnetosphere, the initiation of the increase in flows associated with the SAPS was seen immediately throughout the entire latitudinal extent of the PFISR field-of-view for one of our examples. It has previously been shown that the magnetospheric convection response to IMF changes is rapid and global as seen in the polar-cap ionosphere (Ruohoniemi and Greenwald, 1998; Ridley et al., 1998) and in the dayside equatorial region (Kikuchi et al., 1996). The results here suggest that a prompt global response can also occur within the nightside inner plasma sheet.

Acknowledgments

Research on the grant at UCLA was supported in part by National Science Foundation (NSF) Grant ATM-063931. We are grateful for the opportunity to take advantage of the new capabilities provided by PFISR, and to the NSF CEDAR program for supporting this research. PFISR is operated by SRI International under NSF Cooperative Agreement ATM-0608577. The work of P.C. Anderson was supported in part by NASA Grant NNG05GM25G. We thank J. Weygand at UCLA for providing the propagated IMF and solar wind data.

Referencs

Anderson, P.C., 2004. Subauroral electric fields and magnetospheric convection during the April, 2002 geomagnetic storms. Geophys. Res. Lett. 31, L11801.

Anderson, P.C., Hanson, W.B., Heelis, R.A., Craven, J.D., Baker, D.N., Frank, L.A., 1993. A proposed production model of rapid subauroral ion drifts and their relationship to substorm evolution. J. Geophys. Res. 98, 6069.

Anderson, P.C., Carpenter, D.L., Tsuruda, K., Mukai, T., Rich, F.J., 2001. Multisatellite observations of rapid subauroral ion drifts (SAID). J. Geophys. Res. 106, 29,585.

Angelopoulos, V., Kennel, C.F., Coroniti, F.V., Kivelson, M.G., Pellat, R., Kivelson, M.G., Walker, R.J., Russell, C.T., Baumjohann, W., Feldman, W.C., Gosling, J.T., 1994. Statistical characteristics of bursty bulk flow events. J. Geophys. Res. 99, 21,257.

Angelopoulos, V., et al., 1996. Multipoint analysis of a bursty bulk flow event. J. Geophys. Res. 101, 4967.

Burke, W.J., Maynard, N.C., Hagan, M.P., Wolf, R.A., Wilson, G.R., Gentile, L.C., Gussenhoven, M.S., Huang, C.Y., Garner, T.W., Rich, F.J., 1998. Electrodynamics of the inner magnetosphere observed in the dusk sector by CRESS and DMSP during the magnetic storm of June 4–6, 1991. J. Geophys. Res. 103, 29,399–29,418.

Chen, M.W., Wang, C., Schulz, M., Lyons, L.R., 2007. Solar-wind influence on MLT dependence of plasma sheet conditions and their effects on storm time ring current formation. Geophys. Res. Lett. 34, L14112.

de la Beaujardière, O., Lyons, L.R., Ruohonmiemi, J.M., Friis-Christensen, E., Danielsen, C., Rich, F.J., Newell, P.T., 1994. Quiet-time intensifications along the poleward auroral boundary near midnight. J. Geophys. Res. 99, 287.

Elphic, R.C., Thomsen, M.F., Borovsky, J.E., McComas, D.J., 1999. Inner edge of the electron plasma sheet: empirical models of the boundary location. J. Geophys. Res. 104, 22.679.

Erickson, G.M., Spiro, R.W., Wolf, R.A., 1991. The physics of the Harang discontinuity. J. Geophys. Res. 96, 1633.

Fejer, B.G., Scherliess, L., 1995. Time-dependent response of equatorial ionospheric electric fields to magnetospheric disturbances. Geophys. Res. Lett. 22, 851–854.

Foster, J.C., Burke, W.J., 2002. SAPS: A new categorization for subauroral electric fields. Eos Trans. AGU 83 (36), 393.

Foster, J.C., Vo, H.B., 2002. Average characteristics and activity dependence of the subauroral polarization stream. J. Geophys. Res. 107 (A12), 1475.

Foster, J.C., Erickson, P.J., Lind, F.D., Rideout, W., 2004. Millstone Hill coherent-scatter radar observations of electric field variability in the sub-auroral polarization stream. Geophys. Res. Lett. 31, L21803.

Galperin, Y., Ponomarev, V.N., Zosimova, A.G., 1974. Plasma convection in the polar ionosphere. Ann. Geophys. 30, 1–7.

Goldstein, J., Burch, J.L., Sandel, B.R., 2005. Magnetospheric model of subauroral polarization stream. J. Geophys. Res. 110, A09222.

Heinselman, C., Nicolls, M.J., 2008. A Bayesian approach to electric field and E-region neutral wind estimation with the Poker Flat Advanced Modular Incoherent Scatter Radar. Radio Sci., 43, RS5013, doi:10.1029/2007RS003805.

Kikuchi, T., Lühr, H., Kitamura, T., Saka, O., Schlegel, K., 1996. Direct penetration of the polar electric field to the equator during a DP 2 event as detected by the auroral and equatorial magnetometer chains and the EISCAT radar. J. Geophys. Res. 101 (A8), 17,161–17,173.

Korth, H., Thomsen, M.F., Borovsky, J.E., McComas, D.J., 1999. Plasma sheet access to geosynchronous orbit. J. Geophys. Res. 104, 25,047.

Korth, A., Friedel, R.H.W., Mouikis, C.G., Fennell, J.F., Wygant, J.R., Korth, H., 2000. Comprehensive particle and field observations of magnetic storms at different local times from the CRRES spacecraft. J. Geophys. Res. 105 (A8), 18,729–18,740.

Kozyra, J.U., Jordanova, V.K., Borovsky, J.E., Thomsen, M.F., Knipp, D.J., Evans, D.S., McComas, D.J., Cayton, T.E., 1998. Effects of a high-density plasma sheet on ring current development during the November 2–6, 1993, magnetic storm. J. Geophys. Res. 103 (A11), 26,285–26,305.

Lyons, L.R., 2000. Geomagnetic disturbances: characteristics of, distinction between types, and relations to interplanetary conditions. J. Atmos. Sol.-Terr. Phys. 62, 1087.

Lyons, L.R., Nagai, T., Blanchard, G.T., Samson, J.C., Yamamoto, T., Mukai, T., Nishida, A., Kokubun, S., 1999. Association between GEOTAIL plasma flows and auroral poleward boundary intensifications observed by CANOPUS photometers. J. Geophys. Res. 104, 4485.

Oksavik, K., Greenwald, R.A., Ruohoniemi, J.M., Hairston, M.R., Paxton, L.J., Baker, J.B., H., Gjerloev, J.W., Barnes, R.J., 2006. First observations of the temporal/spatial variation of the sub-auroral polarization stream from the SuperDARN Wallops HF radar. Geophys. Res. Lett. 33, L12104.

Rees, M.H., 1963. Auroral ionization and excitation by incident energetic electrons. Planet. Space Sci. 11, 1209.

Ridley, A.J., Lu, G., Clauer, C.R., Papitashvili, V.O., 1998. A statistical study of the ionospheric convection response to changing interplanetary magnetic field conditions using the assimilative mapping of ionospheric electrodynamics technique. J. Geophys. Res. 103, 4023.

Rowland, D.E., Wygant, J.R., 1998. Dependence of the large-scale, inner magnetospheric electric field on geomagnetic activity. J. Geophys. Res. 103, 14,959–14,964.

Ruohoniemi, J.M., Greenwald, R.A., 1998. The response of high-latitude convection to a sudden southward IMF turning. Geophys. Res. Lett. 25, 2913.

Southwood, D.J., Wolf, R.A., 1978. An assessment of the role of precipitation in magnetospheric convection. J. Geophys. Res. 83, 5227.

Spiro, R., Heelis, R., Hanson, W., 1979. Rapid subauroral ion drifts observed by atmosphere explorer C. Geophys. Res. Lett. 6 (8), 657–660.

Vasyliunas, V.M., 1968. A survey of low energy electrons in the evening sector of the magnetosphere with OGO -1 and OGO-3. J. Geophys. Res. 73, 2839.

Wang, C.-P., Lyons, L.R., Angelopoulos, V., Larson, D.E., McFadden, J., Frey, S., Auster, U., Magnes, W., 2008. THEMIS observations of penetration of the plasma sheet into the ring current region during a magnetic storm. Geophys. Res. Lett., 35, L17S14, doi:10.1029/2008GL033375.

Weimer, D.R., 2004. Correction to "Predicting interplanetary magnetic field (IMF) propagation delay times using the minimum variance technique". J. Geophys. Res. 109, A12104.

Weimer, D.R., Ober, D.M., Maynard, N.C., Collier, M.R., McComas, D.J., Ness, N.F., Smith, C.W., Watermann, J., 2003. Predicting interplanetary magnetic field (IMF) propagation delay times using the minimum variance technique. J. Geophys. Res. 108.

Wolf, R.A., 1983. The quasi-static (slow-flow) region of the magnetosphere. In: Carovillano, R.L., Forbes, J.M. (Eds.), Solar–Terrestrial Physics. D. Reidel Publication Co., Norwell, MA, p. 303.

Wolf, R.A., Spiro, R.W., Sazykin, S., Toffoletto, F.R., 2007. How the Earth's inner magnetosphere works: an evolving picture. J. Atmos. Sol.-Terr. Phys. 69, 288.

Yeh, H.-C., Foster, J.C., Rich, F.J., Swider, W., 1991. Storm time electric field penetration observed at mid-latitude. J. Geophys. Res. 96 (A4), 5707–5721.

Zou, S., Lyons, L.R., Nicolls, M.J., Heinselman, C.J., 2008. PFISR observations of strong azimuthal flow bursts in the ionosphere and their relation to nightside auroras. J. Atmos. Sol.-Terr. Phys., 2008, doi:10.1016/j.jastp.2008.06.015.

Zesta, E., Lyons, L., Wang, C.-P., Donovan, E., Frey, H., Nagai, T., 2006. Auroral poleward boundary intensifications (PBIs): their two-dimensional structure and associated dynamics in the plasma sheet. J. Geophys. Res. 111, A05201.